ELSEVIER

Journal of Nuclear Materials 305 (2002) 112–123

journal of nuclear materials

www.elsevier.com/locate/jnucmat

Size effect studies of the creep behaviour of a pressure vessel steel at temperatures from 700 to 900 °C

Klaus Krompholz *, Dietmar Kalkhof

Nuclear Energy and Safety Department, Paul Scherrer Institut, CH-5232 Villigen PSI, Switzerland

Received 19 April 2002; accepted 2 July 2002

Abstract

The study of size and scale effects in plastic flow and failure is of great importance for the evaluation of the pressure vessel behaviour in severe accidents. The forged reactor pressure vessel material 20MnMoNi55, material number DIN 1.6310 (heat number 69906) was subjected to creep investigations under constant tension load using geometrically similar smooth specimens covering a scaling factor of 4. The tests were performed at 700, 800 and 900 °C in an inert atmosphere. The temperatures cover the phase transformation regime. The mechanical stress varied from 10 to 30 MPa, depending on the temperatures. The creep curves and characteristic data are size dependent to a varying degree, depending on the stress and temperature level. The size effect is largest at 700 °C at the lowest stress level and it implies that the above mentioned times are considerably longer for the small specimens. With increasing stress the size of the effect decreases and at the highest stress a reversal of the effect may occur. The type of fracture is strongly temperature dependent.

1. Introduction

The investigations were performed in the framework of the Euratom EU4 project Reactor Vessel Integrity in Severe Accidents (REVISA) dealing with the reactor pressure vessel behaviour under postulated accidental strain and temperature conditions. One topic was the size effect on deformation and fracture of families of differently shaped specimens. For creep testing the reactor pressure vessel steel 20MnMoNi55 was selected. The specimen fabrication was performed according to an extended plan of specimen drawing. This contribution deals with the creep–rupture test results obtained on two different specimen sizes of smooth creep test specimens at 700, 800 and 900 °C, respectively. This investigation was felt to be necessary in view of the results of previous creep studies.

A review of experiments on similarity and size effects in uniaxial creep of smooth, unnotched specimens has been performed [1], while investigations on notched specimens in creep were performed elsewhere [2]. It is important to note that primarily the influence of the specimen diameter (or plate thickness) was considered in these studies. In a few studies also the effect of gauge length was investigated but experiments exclusively concerned with geometrically similar specimens are rather scarce. In most cases the parameters chosen to characterise the creep behaviour were the secondary creep rate (steady-state creep stage), the time to rupture, and the percentage elongation at fracture.

In a variety of studies [2–4] an increase of specimen diameter caused an increase of the rupture time for brittle steels and nickel base alloys, but non-monotonic responses also were found. Ductile steels generally exhibit no dependence on the diameter, but the opposite was also observed. The secondary creep rate was usually decreased with increasing diameter but, depending on microstructures and temperatures, it sometimes increased or showed no change. In a lot of cases not only

* Corresponding author. Tel.: +41-56 3102 300; fax: +41-56 3102 199.

E-mail address: klaus.krompholz@psi.ch (K. Krompholz).

0022-3115/02/$ - see front matter
PII: S0022-3115(02)01029-2

insufficient geometrical similarity was present, but also environmental action, especially surface oxidation in air but also decarburisation in noble gas introduced pseudo effects. Also the misalignment of the load (bending forces) caused an apparent size effect. Beyond these effects statistical aspects of defects in the material volumes or intrinsic material properties were proposed as explanations.

It can be concluded that the available experimental data on the issue of size effects in smooth specimens is quite defective. A single general trend in the response under a change of dimensions is not found and interpretations relate to technological effects (e.g. surface hardening) or adverse testing conditions. Explanations referring to a real material behaviour remain on the level of plausibility.

The creep–rupture results presented in this study refer to geometrically similar smooth specimens with circular cross-section (5 and 20 mm diameter) and a gauge length five times the diameter, thus the geometrical scaling factor is four. Because the knowledge of the material scatter and possible positional influences on the test results are of most importance for the discussion of the results a preliminary study of the material homogeneity for the size effect investigations was undertaken [5].

Prior to the creep tests the temperature regime of the α- to γ-phase transformation was determined by different methods as well as the scale oxidation behaviour of this material. These investigations were necessary to define the temperature levels for the creep–rupture tests, which should be below, within and above the phase transformation regime; also environmental effects should be minimised during the testing.

2. Phase transformation regimes

It is well known that this ferritic material undergoes a phase transformation from the cubic body centred lattice (α-phase) to the cubic face centred lattice (γ-phase) at elevated temperatures. For this type of material, the phase transformation does not take place at one temperature, but there exists a temperature regime in which the two different phases coexists. In this regime the material behaves like a compound material. The phase transformation was studied by means of the determination of the electrical resistivity as well as dilatometric measurements, which allows very accurate measurements of changes in the response characteristics, which are due to the phase transformation. The temperature range of the phase transformation was determined for three different materials, the material under investigation, the Russian pressure vessel steel 15Kh2MFA and the French pressure vessel material 15CD910. The results of the measurements are reported in Table 1. It can be seen that the selected temperature of 700 °C for the creep tests is within the range of the phase transformation which starts at about 690 °C during heating. Even the temperature of 800 °C is completely in the regime of the phase transformation. The temperature regime could be determined accurately by means of the dilatometric measurements. From this the linear coefficient of thermal expansion was determined by the following equations

Table 1
Phase transformation of the pressure vessel steels

Material	Heating T/K (T/°C)	Cooling T/K (T/°C)
20MnMoNi55	962–1115 (689–842)	Not determined
15Kh2MFA	1045–1150 (772–877)	1060–930 (787–657)
15CD910	1035–1120 (762–847)	1056–970 (783–697)

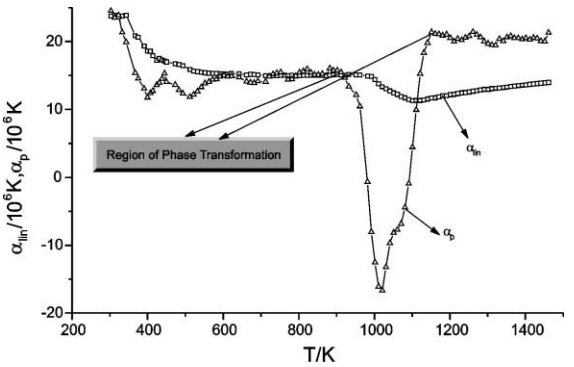

Fig. 1. Regime of phase transformation for the pressure vessel steel 20MnMoNi55 obtained by dilatometric measurements. Linear and physical coefficient of thermal expansion.

$$\alpha_{\text{lin}} = \frac{l - l_0}{l_0(T - T_0)}, \tag{1}$$

while the physical (incremental) coefficient of thermal expansion is given by

$$\alpha_{\text{phys}} = \frac{\mathrm{d}l}{l_0\,\mathrm{d}T}. \tag{2}$$

These coefficients are presented in Fig. 1 for the material under investigation. The physical coefficient of thermal expansion delivers the best possibility to determine the transformation temperatures.

3. Experimental details of the creep tests

For these experiments the pressure vessel material 20MnMoNi55 was used, which is described elsewhere [1]. The chemical composition is given in Table 2. One position within the plates delivered yield stresses and ultimate tensile stresses larger than those observed from other positions combined with reduced ductility. This

Table 2
Chemical composition of 20MnMoNi55 in wt%

C	Si	Mn	P	S	Cr	Ni	Mo	Sn	Co	Ta	Cu	N	Al	V
0.20	0.28	1.30	0.9	0.002	0.11	0.65	0.47	0.006	0.01	0.005	0.030	0.005	0.028	0.005
0.23	0.33	1.22		0.005		0.71	0.44		0.02		0.036			

had to be considered in the interpretation of the results. Two specimen types have been investigated under creep conditions, the specimen type C1 (small specimen, 5 mm diameter) and a geometrically similar specimen type C2 (large specimen, 20 mm diameter), see Fig. 2. For both specimens the gauge length to diameter ratio is 5. During the course of the testing at 800 °C, some specimens fractured outside the gauge length. Therefore, additional modified specimens were machined with enlarged gripping rims and enforced sections outside of the gauge length without affecting the gauge section dimensions.

The creep tests were performed in a flowing argon atmosphere within test chambers. The argon flow rate was about 30 l/h. The temperature was measured by means of Pt/Pt10Rh thermocouples at the specimen. The temperature was reached by means of three-zone resistance furnaces.

For creep testing the creep machines of Mohr/Federhaff/Losenhausen with a maximum load capacity of 40 kN were applied. The respective loading was performed with a single beam of balance, where the constant weight was brought to a plate after a heating phase and isothermal conditioning of about 6–8 h. During fracture the plate with the load comes into contact with a bolt, which switches off the clock.

For the determination of the elongation, inductive extensometers of the type D25.WA.1 of HBM (Hottinger Baldwin Messtechnik, Darmstadt), were used. For the specimen C1 a maximum elongation of 50 mm could be measured, while for the specimen C2 the measurable elongation was 200 mm.

The data were stored by a recorder as well as taken as data files in a CATMAN procedure delivered by HBM.

After putting the loads on the plates, the plate support was removed slowly. The test procedure followed the ASTM E 139-95 recommendations [6].

In addition to the continuous measurement of the elongation during the test, the area reduction and the elongation at fracture were determined from the broken specimens.

4. Data definition and reduction

The tests were performed under constant load. The initial stress is calculated according to

$$\sigma_0 = \frac{F_0}{S_0}, \tag{3}$$

where F_0 represents the weight (load), which is put on the load plate of the creep machine, and S_0 is the respective initial cross section of the specimen. For the engineering creep curve the stress is considered to be constant.

For the creep curves the relative elongation of the specimen versus time is considered.

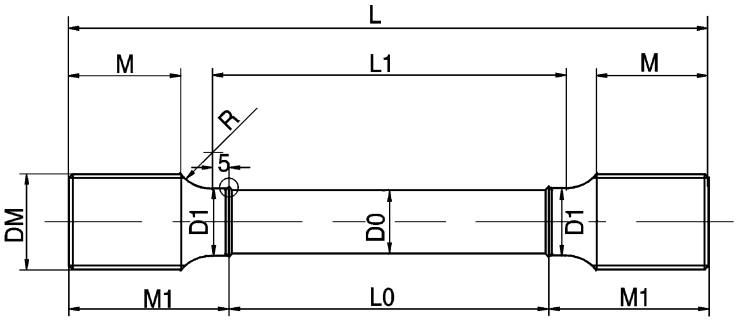

Type	L/mm	L1/mm	L0/mm	M/mm	M1/mm	D0/mm	D1/mm	DM/mm	R/mm
C1	67	35	25	12	21	5	6	10	4
C2	200	110	100	35	50	20	22	30	12

Fig. 2. Specimen type C1 (small specimen) and C2 (large specimen).

The total elongation under creep conditions can be expressed as

$$\varepsilon = \varepsilon_e + \varepsilon_i + \varepsilon_f, \tag{4}$$

where ε_e is the elastic strain, ε_i the initial plastic strain and ε_f the creep strain. Under normal conditions the creep contribution is formed by the plastic strain contribution, and the elastic contribution can be neglected. From these tests the technical creep curves have the following functions

$$\varepsilon_p = \varepsilon_i + \varepsilon_f. \tag{5}$$

$$\varepsilon_p = f(\sigma_0, t), \quad \text{with the technical strain} \tag{6}$$

$$\varepsilon_p = \frac{\Delta l}{l_0}, \tag{7}$$

where

$$\Delta l = l - l_0, \tag{8}$$

where l_0 is the initial length. From this curve the slope of the steady-state creep is determined by determining the derivative of the curve in the range of secondary creep. This is important for the determination of Norton's creep law [7]

$$\frac{d\varepsilon}{dt} = K\sigma_0^r, \tag{9}$$

where K and r are constants, which remain approximately unchanged. In addition to Norton's creep law, the stress to rupture behaviour is described by

$$\sigma_0 = K_1 t_f^l, \tag{10}$$

where K_1 and l are constants and t_f is the time to fracture. Eq. (10) describes the time to rupture relationship and is used for a lifetime determination. For design rules the parameter t_f is replaced in Eq. (10) by the times for 5% and 15% strain. The reduction of area was evaluated according to

$$Z_u = \frac{S_0 - S}{S_0}, \tag{11}$$

where S_0 is the initial cross section, and S is the cross section after fracture.

5. Experimental results and discussion

5.1. Creep curves

The total strain versus time is represented in Cartesian coordinates. A variety of specimens have been tested at temperatures of 700, 800 and 900 °C. Different stress levels ranging from 10 to 30 MPa were used.

Figs. 3–5 show the creep curves obtained at 700, 800 and 900 °C, respectively. It is obvious from the comparison of the different creep curves that there is a clear size effect, which is not unique, in agreement with literature. The following qualitative observations can be made.

700 °C, see Fig. 3: At high stresses of 30 MPa there is practically no difference in the strain–time curve of the C1 and C2-specimens (single measurements only), except below 10% strain. However, the strain at fracture (endpoints of the creep curve) is lower for the large specimens. For the stress level of 25 MPa two tests for each specimen type were done. In comparison to the C1-specimens the curve of the larger C2-specimens are shifted to longer times (i.e. smaller secondary creep rates) and yield somewhat smaller strain at fracture but larger times to fracture. A significant effect of size is found for the tests at 15 MPa. Whereas the small

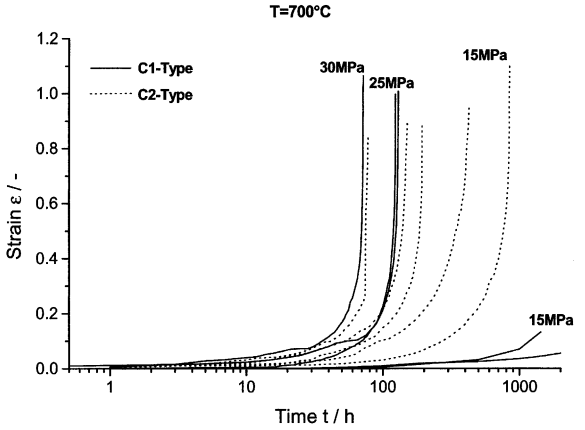

Fig. 3. Creep curves strain versus time for the specimens type C1 and C2, 700 °C.

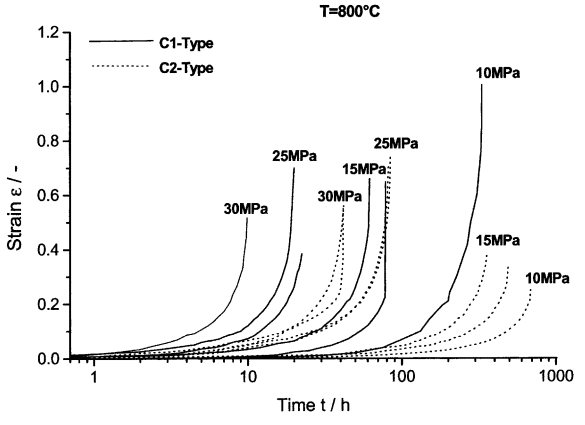

Fig. 4. Creep curves strain versus time for the specimens type C1 and C2, 800 °C.

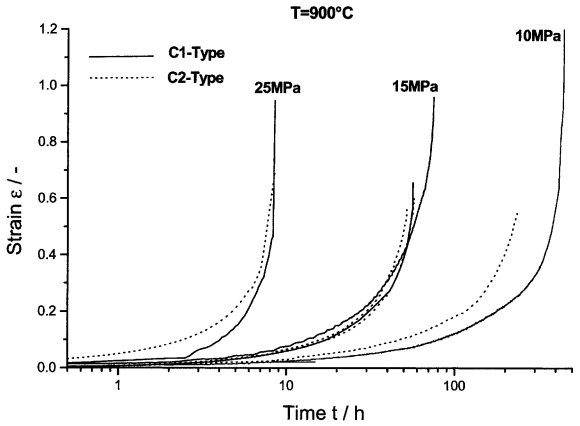

Fig. 5. Creep curves strain versus time for the specimens type C1 and C2, 900 °C.

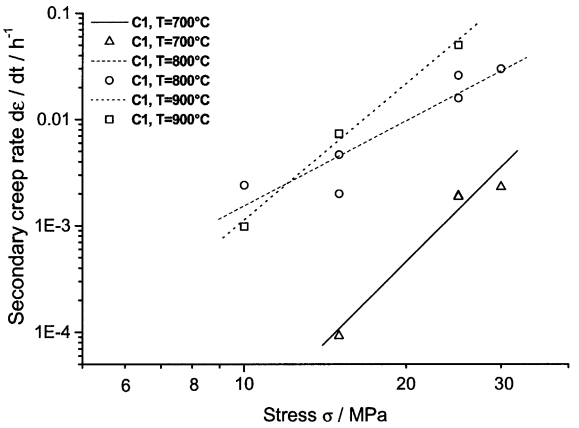

Fig. 6. Steady-state creep rate versus stress for the specimens type C1.

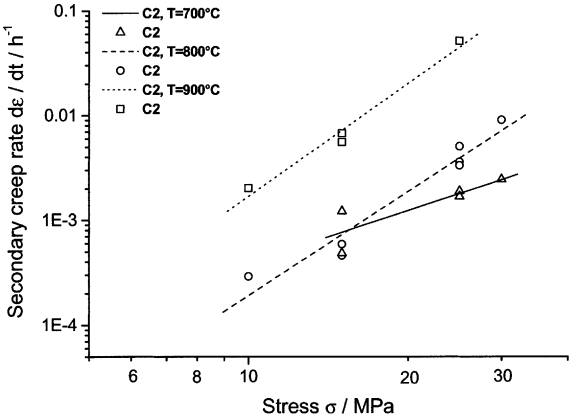

Fig. 7. Steady-state creep rate versus stress for the specimens type C2.

C1-specimens have rather low creep rate and did not fail after 1434 and 2700 h, respectively, the corresponding large C2-specimens showed a considerably larger creep rate and failed after 427 and 845 h, respectively.

800 °C, see Fig. 4: At this temperature, only two stress levels (25 and 15 MPa) allow size effect considerations. Fig. 4 shows that the creep curves for the large specimens (type C2) have much smaller creep rates and longer times to fracture. At 25 MPa the strains at fracture show some scatter, and a size influence cannot be detected. At 15 MPa the strain at fracture is fairly reproducible for both sizes, and the large specimens yield only about 30% strain instead 65% for the small ones.

900 °C, see Fig. 5: For the three stresses (10, 15 and 25 MPa) size effect considerations are possible, but only for the 15 MPa level a repeat of the test was done. Within the scale of the Cartesian representation of the creep curves in Fig. 5, the results are quite reproducible. For the stress levels of 15 and 25 MPa the creep curves almost agree. Whereas times to rupture agree (times are sufficiently short), the strain at fracture (endpoints of the curves) are consistently smaller for the large specimens. For the low stress level of 10 MPa, however, the mean strain rate of the large specimens is clearly larger than for the small specimens (single measurement only), time to rupture and strain at fracture are a little smaller for the large specimens.

5.2. Minimum creep rate

Figs. 6 and 7 show the creep rupture behaviour of the specimens of type C1 and C2 derived from the respective creep curves. Plotted are the steady-state creep rates versus stress on a double logarithmic scale. The minimum creep rate was determined by inspection of the creep curves and is defined by the slope of the straight section, if existent, or by the slope of the turning point in the creep curve. Fig. 6 shows the minimum creep rate versus stress of the specimen type C1, while Fig. 7 shows the same for the specimens of type C2. Linear regression curves seem to fit the data reasonably well. Therefore, from these plots the parameters of Norton's creep law, see Eq. (9), can be determined using the logarithmic form

$$\log \dot{\varepsilon} = \log K + r \log \sigma_0. \tag{12}$$

Thus the slope of the regression lines corresponds to Norton's creep exponent. It is obvious from Figs. 6 and 7, that at 800 °C the slopes for the two specimen sizes are nearly the same and only the creep parameter K is affected by a change of size: the smaller specimens give a larger K-parameter, i.e. larger minimum creep rate in the whole stress range.

At 900 °C, after complete austenitisation of the specimens, the smaller specimens of type C1 yield a slightly larger slope (larger creep exponent) than the

large specimens of type C2 and an intersection of the regression lines within the stress range is observed. Thus, at low stresses the small specimens yield smaller minimum creep rates whereas at larger stresses larger rates are observed. In comparison to the results at 800 and 700 °C, however, the size effect is relatively small for this quantity. This is evident because the times to fracture are small.

At 700 °C the slope of the regression line for the small specimens type C1 is clearly larger than at 800 and 900 °C. For the large specimens C2, however, a rather small slope is found, i.e. an untypical Norton-exponent of nearly one, while for all other cases the exponents are $3.5 < r < 5.1$. Also an intersection of the two regression lines is observed. This implies that the K-parameter of the small specimens type C1 is much smaller than for the large specimens type C2. this crossover implies that the smaller specimens yield smaller minimum creep rates at lower stresses than the large ones (e.g. at 15 MPa the difference is almost a factor of 10) and this behaviour is reversed when large stresses are applied. Thus, at 700 °C and small stresses minimum creep rate data obtained from small specimens (5 mm diameter) yield non-conservative deformation rate predictions for large specimens and/or real structures.

5.3. Time to 5% and 15% strain

For design codes the time to 5% and 15% elongation is of importance. For that reason Figs. 8 and 9 show the relevant plots of stress versus time to 5% and 15% elongation in the double logarithmic scale, respectively. The situation for the time to 5% and 15% elongation is nearly the same as for the plots of stress versus time to rupture. The regression lines for the specimens of type C1 are given in full lines, while the regression lines for the large specimens of type C2 are shown in dotted lines. The size effect for these types of specimens is obvious.

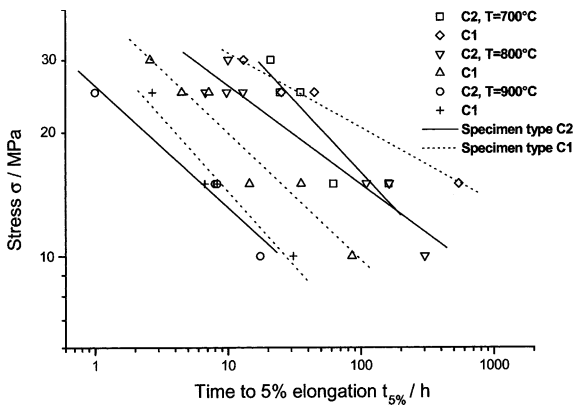

Fig. 8. Stress versus time to 5% elongation for the specimens C1 and C2.

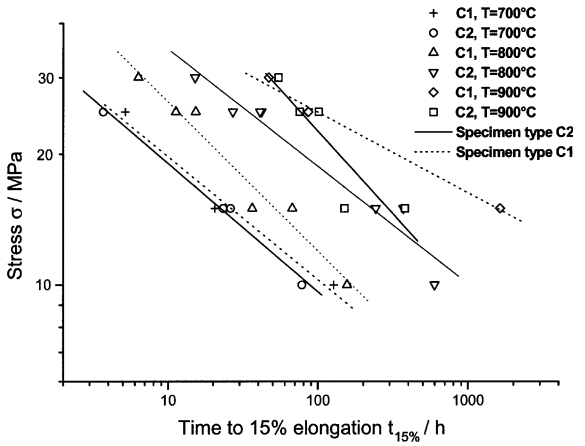

Fig. 9. Stress versus time to 15% elongation for the specimens C1 and C2.

700 °C: The data of the small C1-specimens for the very low stress of 15 MPa are estimated from the measured strain–time curves available up to 1434 and 2700 h, respectively. For low stresses the time to 5% and 15% strain is considerably lower for the small C1-specimens, while for high stresses a reversed response is found; this qualitative trend simply reflects the trend observed for the minimum creep rate at this temperature.

800 °C: At all applied stress levels the small specimens deliver considerably shorter times than the large ones and thus yield conservative results, in agreement with the trend for the minimum creep rate. The situation may reverse at high stress levels where a crossover is suggested if linear regression lines are extrapolated.

900 °C: Within the stress range investigated the differences in the time–strain limits $t_{5\%}$ and $t_{15\%}$ for the small and the large specimens are relatively small but small specimens seem to yield slightly longer times. As a general observation, the change in specimen size (from 5 to 20 mm diameter) results in an increase or decrease of the time–strain limits for $t_{5\%}$ and $t_{15\%}$, depending on the stress and temperature level. Within the tested parameter range the size influence is clearly less than a factor of 10.

5.4. Time to rupture

As was shown before, the time–strain limits $t_{5\%}$ and $t_{15\%}$ and the minimum creep rate are qualitatively well correlated. This is expected since the minimum creep rate is associated with relatively small strain levels. This may not be so for the time to rupture if a pronounced tertiary creep range exists. The time to rupture behaviour is derived from the plots of the stress versus time to rupture, which are measured either by the external time counter or by the internal clock of the data acquisition. Fig. 10 shows the stress versus time to rupture for the specimens of type C1, and type C2 for the three

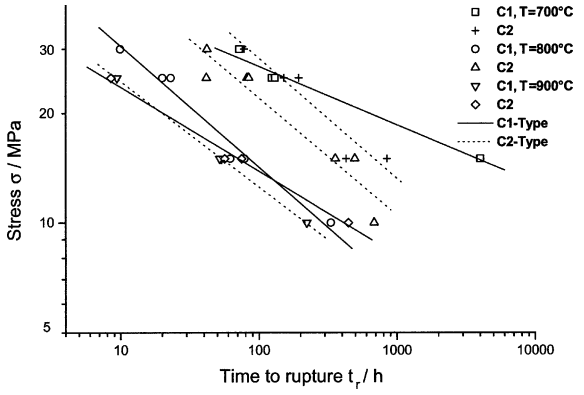

Fig. 10. Stress–rupture behaviour of the specimens type C1 and C2.

temperatures. Both plots are presented in a double logarithmic scale. The corresponding data are given in the tables of the appendices. For the small specimens at 700 °C and a stress level of 15 MPa, the time to rupture was assumed to be 4000 h, a lower limit. Inspection of Fig. 10 definitively shows that the trend found for the time–strain limits $t_{5\%}$ and $t_{15\%}$ are also obtained for the time to rupture.

At *700 °C:* Small specimens yield significantly longer time to rupture at low stress levels than the large specimens, and at larger stress levels, a reverse behaviour is seen.

At *800 °C:* Generally small specimens yield shorter times to rupture, but extrapolation to large stresses suggests a reversal of the behaviour.

At *900 °C:* Again, differences are smallest. At small stresses the small specimens yield somewhat larger times to rupture, but a reversal of response occurs about 25 MPa.

The qualitative behaviour already found for the minimum creep rate transfers also to the creep–rupture time (using the rule, large minimum creep rates are equivalent with small times to rupture).

5.5. Elongation at fracture

It should be mentioned that the elongation at fracture A_u was measured at room temperature by joining the halves of the broken specimens. Thus, these values do not necessarily agree with the final strain values in the creep curves, but it is expected that the differences are sufficiently small such that trends agree.

At 700 °C for the small C1-specimens only one test is available at 30 MPa, but at 25 MPa two tests were done. For these three tests the measured elongation agree reasonably well with the final strain of the creep curves. However, at the lowest stress level (15 MPa) two tests were done without rupture. The first test was terminated after 1434 h without fracture, the second one is running about 2400 h reaching a strain of 6.2% without fracture. The elongation at fracture agree reasonably well with the final strains taken from the creep curves.

At 800 °C the small C1-specimens appear to yield an extreme scatter at 15 and 25 MPa, see Fig. 11. The elongation of the small specimens seems to be stress independent, but the experimental basis is too meager. A considerable difference is seen in the stress dependence of the fracture elongation between the small and the large specimens at this temperature. Whereas at high stresses the two sizes have no influence on the average elongation, the elongation of the small specimens is almost two times larger than the large specimens at the small stress level of 15 MPa. A similar trend was observed at 700 °C. However, further tests would be desirable.

At 900 °C all specimens fractured within the gauge length. The elongation at fracture of the small specimens are subject to a considerable scatter at 15 MPa. For the other two stress levels only single measurements were done. This makes the trend assessment of the stress dependence rather uncertain. Nevertheless, below 15 MPa the elongation seems to increase with decreasing stress. These findings agree reasonably well with the final strains of the corresponding creep curves. The elongation at fracture of the large specimens, however, almost does not depend on the applied stress, and again they are in agreement with the final strains in the creep curves. In comparison, the mean values of the elongation of the small specimens are all larger, especially at the very low stress of 10 MPa, the difference amounting to more than a factor of 2.

For documentation some examples of the state of the specimens after fracture are presented in Figs. 12–14. The pictures clarify the difference in the geometry of the specimens as well as the difference of the fracture data. It is obvious from the pictures that the largest necking is

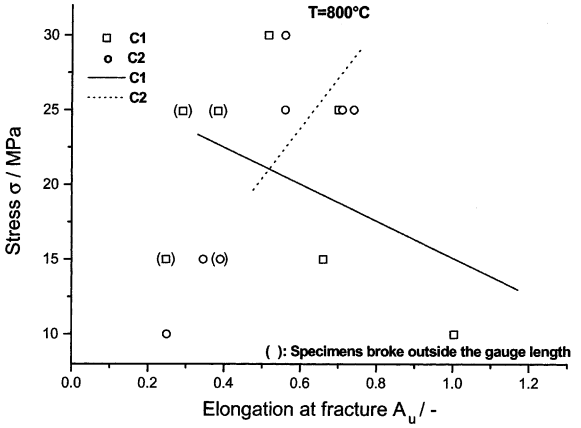

Fig. 11. Stress versus strain to rupture for the specimens type C1 and C2, 800 °C.

Fig. 12. Specimens type C1009, and C2024, $\sigma = 25$ MPa, 700 °C.

Fig. 13. Specimens type C1033, and C2030, $\sigma = 15$ MPa, 800 °C.

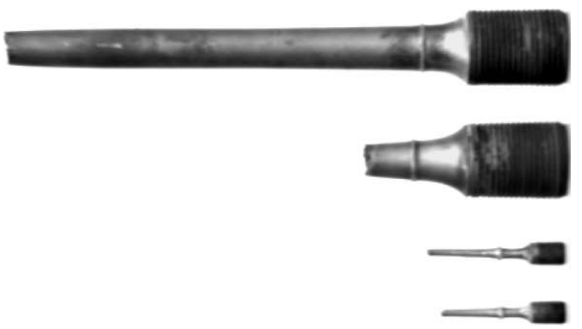

Fig. 14. Specimens type C1001, and C2001, $\sigma = 25$ MPa, 900 °C.

obtained for the specimens tested at 700 °C, see Fig. 12, while at 800 and 900 °C the fracture is more brittle in spite of the higher temperature and the larger contributions of the austenitic phase. Prior to the discussion of the area reduction at fracture, it is reasonable to discuss the meridional profiles of typical small and large specimens at the three temperatures. The eye-catching difference is to be seen in the fracture modes.

At 700 °C, see Fig 12, both the large and the small specimens have a large reduction of area and a pronounced transition from the neck to the gauge marking, which implies a non-uniform change of the cross section along a long part of the gauge section. This is even more pronounced for the small specimen. According to DIN 50118 [8], this mode belongs to fracture type 3.

At 800 °C, the cross section reduction is rather uniform along the gauge length, both for the large and the small specimen, and the area reduction at the fractured section is clearly smaller than at 700 °C, see Fig. 13. However, the small specimen has a considerably larger elongation and reduction of area. This mode corresponds to fracture type 2.

At 900 °C, it appears that the uniformity in the gauge section is slightly less than at 800 °C for the large specimens, see Fig. 14. This is even more pronounced for the small specimens. Obviously both for the small and the large specimens the area reduction is clearly smaller than at 700 °C.

It may be noted that the high-temperature induced creep can be observed in the whole specimen, as may be seen from the conical deformation of the threaded ends. It should be mentioned that the statement of ASTM E139 [6] that size independence is only violated if the material is not sound or subjected to appreciable surface corrosion cannot hold for this type of material.

5.6. Temperature dependence of elongation at fracture and reduction of area

The stresses of 15 and 25 MPa are common for all temperatures under investigation. Figs. 15–18 show the temperature dependence of the elongation at fracture and the reduction of area. For the low stress of 15 MPa for the specimen of type C1 the reduction of area and the elongation at fracture are not available because the

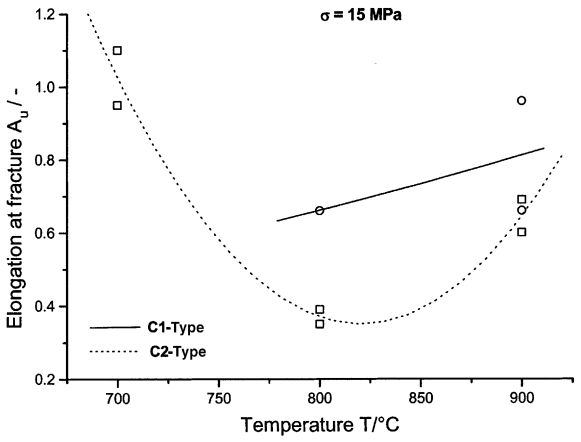

Fig. 15. Temperature dependence of the elongation at fracture for a stress of 15 MPa.

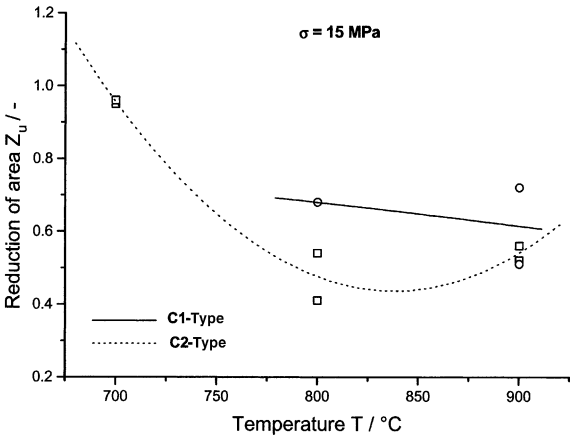

Fig. 16. Temperature dependence of the reduction of area for a stress of 15 MPa.

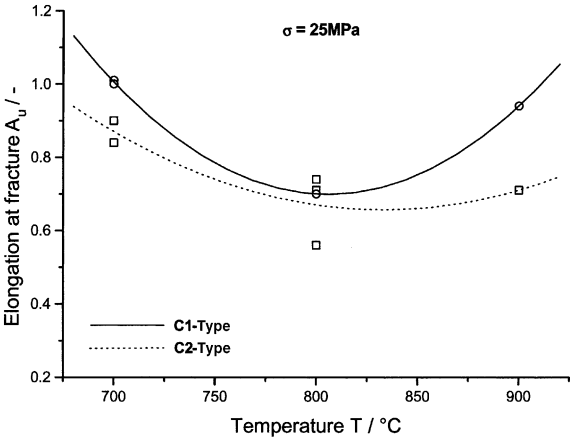

Fig. 17. Temperature dependence of the elongation at fracture for a stress of 25 MPa.

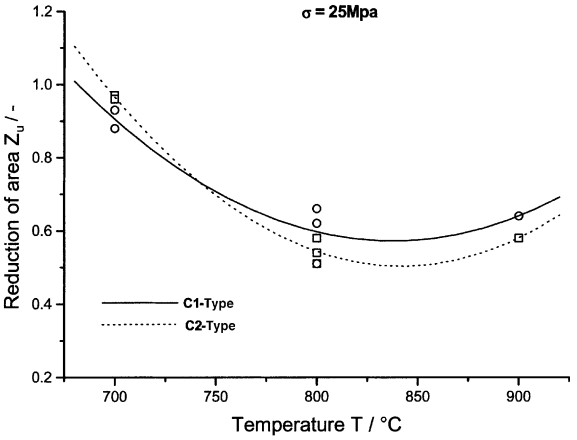

Fig. 18. Temperature dependence of the reduction of area for a stress of 25 MPa.

tests were either terminated before fracture or are still running. Therefore, the regression line for this type of specimen is only valid between 800 and 900 °C, see Figs. 15 and 16. For the large specimens, all data are available and reveal a decrease from the beginning of the phase transformation. The lowest value of the regression parabola is between 825 and 840°, i.e. at the end of the phase transformation regime (689–840 °C). For the stress of 25 MPa the data are available for both types of specimens. It is obvious that the minimum for the elongation at fracture is near 800 °C for the small specimen, while for the large specimen it is shifted towards the upper boundary of the phase transformation regime. For the reduction of area, all data were used, even those that failed outside the gauge length because the data were within a narrow scatter band. For the reduction of area the minimum is found at the boundary of the phase transformation for both types of specimens, see Figs. 17 and 18. Accordingly it may be concluded that the compound material in the interim region between the ferritic and austenitic phase reduces both the reduction of area as well as the elongation at fracture. Unfortunately, the data available for this discussion are rather few and further investigations are recommended.

5.7. Size dependence of time to rupture and regression parameters for minimum creep rate and stress–rupture behaviour

Figs. 19–21 exhibit the time to rupture as a function of diameter of the specimens; the time is plotted in the logarithmic plot while the diameter of the two specimens is represented in a linear scale. It is obvious from the results for the tests at 700 °C that the largest change is found for the small stresses, a behaviour, already discussed. Also, at 900 °C the small specimens are non-conservative with respect to time to rupture. The former considerations reveal the problem in discussing size

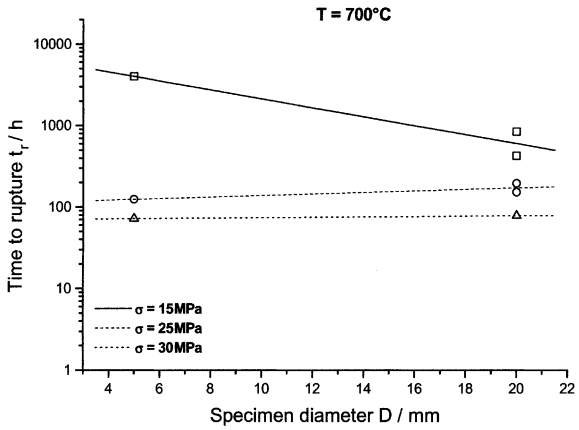

Fig. 19. Time to rupture versus specimen diameter for the specimen C1 and C2, $T = 700$ °C.

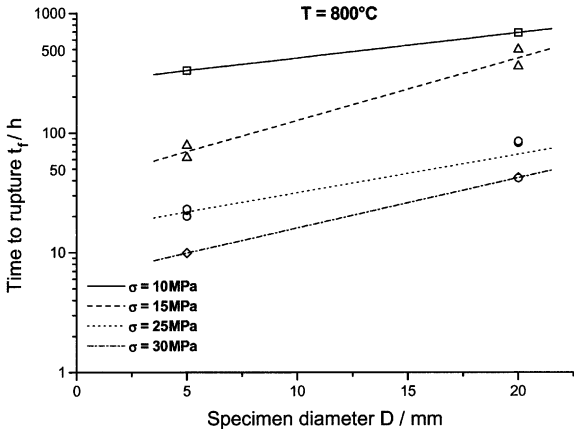

Fig. 20. Time to rupture versus specimen diameter for the specimen C1 and C2, $T = 800$ °C.

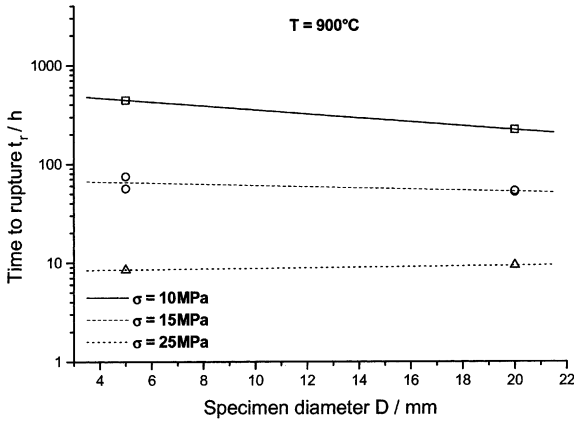

Fig. 21. Time to rupture versus specimen diameter for the specimen C1 and C2, $T = 900$ °C.

effects in creep. Specific considerations are undertaken with respect to the Norton's creep law as well as time to rupture. The last one is important for the stress–rupture behaviour, while Norton's creep law is used for conservative deformation time predictions.

The parameter K_1 and the exponent l of the power law for the stress dependence of the time to rupture, see Eq. (10), as a function of the specimen diameter D are shown in Figs. 22 and 23. Whereas the exponent l is decreasing with size at 700 and 900 °C, it is increasing at 800 °C, where the steel is a compound material in the transition region. On the other hand, the parameter K_1 is increasing with size at 700 and 900 °C, admittedly to rather different degrees, but at 800 °C it is decreasing. For both couples of parameters, it is also seen that the temperature dependence is generally non-monotonic for both sizes but differently, i.e. decreasing, passing a minimum and increasing with temperature or vice versa.

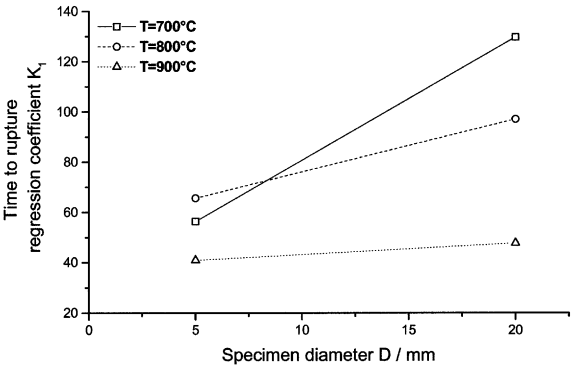

Fig. 22. Shift of the time to rupture regression coefficient K_1 versus specimen diameter for C1 and C2.

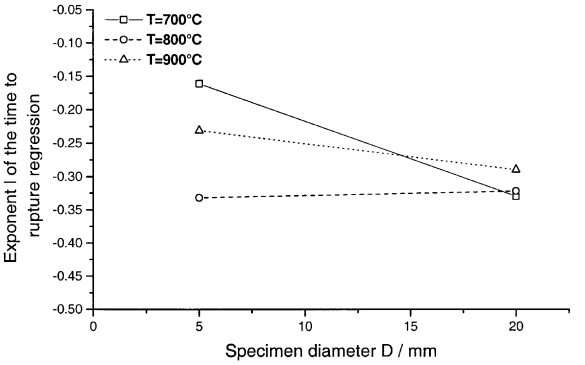

Fig. 23. Exponent of the time to rupture regression versus specimen diameter for C1 and C2.

It was shown that the stress dependence of the secondary creep rate approximately followed Norton's creep law, Eq. (12), and the size dependence of Norton's parameters K and r was discussed in qualitative terms. In Table 3, and Figs. 24 and 25 the size (diameter) influence is shown for the three temperatures.

Whereas the size influence of the Norton-exponent r is rather moderate at 800 and 900 °C, it is extreme at

Table 3
Regression parameters for Norton's law and stress versus time to rupture

Specimen type	T/°C	$K \times 10^8$	r	K_1	l
C1	700	0.0124	5.05	56.27	−0.161
C2	700	857	1.660	129.62	−0.33
C1	800	13.5	3.70	90.37	−0.421
C2	800	1.17	3.95	71.07	−0.253
C1	900	6.34	4.25	40.91	−0.231
C2	900	45.9	3.57	47.63	−0.290

$\dot{\varepsilon} = K\sigma_0^r$, Norton's law; $\sigma_0 = K_1 t_f^l$, initial stress versus time to rupture.

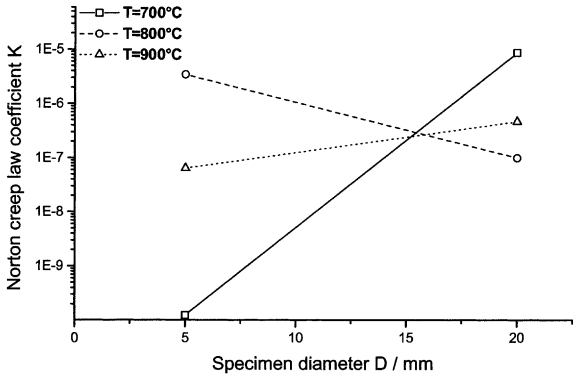

Fig. 24. Coefficient of Norton's creep law versus specimen diameter for C1 and C2.

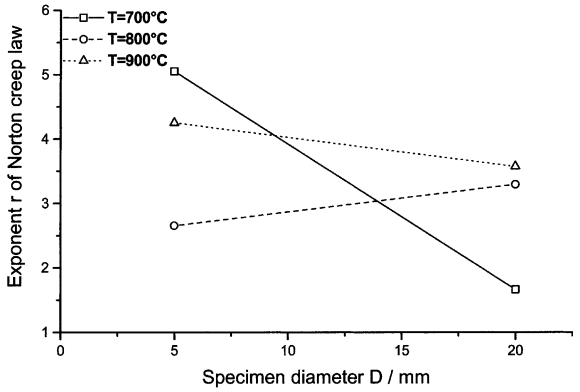

Fig. 25. Exponent of Norton's creep law versus specimen diameter for C1 and C2.

700 °C. This is essentially due to the extraordinarily small exponent for large C2-type specimens see also Fig. 8 (minimum creep rate versus stress at 700 °C). At this temperature, the *K*-parameter shows a rather strong dependence on the diameter. This extreme behaviour requires further investigations. It is obvious that creep is not a size independent physical property of the material. It should be mentioned that creep has to be handled as a function of a variety of parameters, e.g.

$$\varepsilon = f(\sigma_0, T, V, \Delta H), \tag{13}$$

where σ_0 describes the external stress, T the temperature, V the active volume, ΔH the internal energy describing the state of the material. From this point of view, a size independence of the creep phenomena cannot be expected, as mentioned in ASTM E 139-00, note 4 [6]. It should be mentioned that this material may be very sensitive to specimen sizes in the selected temperature regimes, because this type of material is not suitable for this temperature region and these investigations are restricted to accidental temperatures.

5.8. Numerical experimental data

All numerical results from regressions can be found in Table 3.

6. Conclusions

The analysis of the experimental results leads to the following observations and conclusions.

(1) The times to 5% and 15% elongation are size dependent. At 700 °C for the lowest stress (15 MPa) these times are considerably larger by a factor of 10 and 6 for the small specimens of type C1, while for the higher stresses the situation is reversed, but differences are much less (a factor of 1.6 and less for the highest stress of 30 MPa). At 800 °C and all stress levels (15 and 25 MPa) a completely different size influence is found: the small specimens of type C1 yield considerably shorter times to obtain these elongations (factor of 5.5 and 5.9). A reversal of the size influence may be anticipated for higher stresses if linear regression lines are extrapolated. At 900 °C the size influence on the times to 5% and 15% strain within the stress range investigated (10–25 MPa) is relatively small compared to the lower temperatures; at the lowest and highest stress the smaller specimens yield longer times to reach these elongation (ratios between 1.4 and 2.7).

(2) The time to rupture is also size dependent and follows under most test conditions the same tendencies as the times to 5% and 15% strain.

(3) Most tests did not reveal a clear secondary (steady-state) creep stage. In these cases the creep rate at the turning point of the strain versus time diagrams was determined, which corresponds to the minimum creep rate. At 700 °C and the lowest stress level (15 MPa), the average minimum creep rate of the small specimens is a factor of 12 smaller than that of the large specimens; this difference is of significance because it is much larger than the scatter (factor of 2–2.5) of the nominally identical tests at these test conditions. When the stress was increased to 25 and 30 MPa, the tendency appears to be retained, but the differences become smaller (factor of 1.25 and 1.06) with scatter bands of small and large specimens practically overlapping. This result implies that deformation rate predictions at 700 °C for large specimens or structures, which are based on the minimum creep rate results of small specimens at low stress levels, are non-conservative. At 800 °C a very different size influence on the stress dependence of the minimum creep rate is found: at both stress levels investigated (15 and 25 MPa) the small specimens yield a considerably larger minimum creep rate (factor of 6.15 and 5.2 in the average). Finally, at 900 °C the small specimens of type C1 yield at the lowest stress (10 MPa) a smaller minimum creep rate (factor of about 2) than the large

specimens of type C2, and this difference decreases with increasing stress, as expected. Further, the trend of the size influence on the time to rupture is also reflected in the minimum creep rate if the size effect is more than a factor of 2.

(4) The elongation at fracture A_u of the small specimens is larger than that of the large specimens at all temperatures and stress levels, but to a varying degree. In this temperature and stress region, small specimens of type C1 yield mostly non-conservative fracture elongation. It is obvious that at low stress levels this size effect is largest, but the data at 700 °C have not been obtained since the small specimens did not fail yet.

(5) The type of fracture is temperature dependent. At 700 °C both the small specimen as well as the large specimen show a pronounced necking with an extended transition from the neck to the gauge markings. At the higher temperatures the creep is rather uniformly distributed along the whole gauge length with a minor neck formation. Creep deformation is even found in the threaded ends of the specimens at all temperatures.

(6) The material under investigation undergoes a phase transformation in the temperature range of about 690–840 °C from the ferritic α-phase, which is body centred cubic, to the austenitic γ-phase, which is face centred cubic in lattice structure. This phase transformation has taken place in the region of investigation before the start of the creep testing. Thus, applying the rule of balance, at 700 °C about 7.2% of the original ferritic material becomes austenitic, whereas at 800 °C it is about 72.5% and at 900 °C a complete austenitisation (100%) is obtained. Accordingly, the microstructures at the three temperatures are rather different. If microstructure properties and length-scales in relation to the macroscopic geometric length scales determine the size influence, then it is not to be expected that the size effect trends observed at one temperature transfers to another one; this has been indeed observed.

(7) A theoretical explanation or interpretation of the observed size influence is presently beyond the scope of this study. Macroscopic material in homogeneity or orientation effects as well as severe corrosion can be excluded. Therefore, the observed size influence is in contradiction to the statement of ASTM designation E 139 that influences of specimen size can be neglected provided the material is sound or not subjected to appreciable corrosion effects. This is not the case for this material. It suggests itself that some diffusion processes may be responsible for the observed size effect, and these processes are more important in small specimens than in large ones. Thus, if sufficient time is available, such processes become important and size influences due to diffusion may show up. Since creep tests at lower stress levels have longer test duration than at higher stresses, diffusion induced size effects should be more pronounced at the low stress level. This, in fact, has been observed. The qualitative suggestion needs, of course, considerable assessment. From this investigation the following conclusions can be drawn with respect to accident considerations. The region of phase transformation cannot be considered as a step function with creep properties of a ferritic phase below phase transformation and of an austenitic phase above this temperature. Modelling a pressure vessel and using the data from usual creep tests may deliver non-conservative results. Data from tests performed on scaled down structures, e.g. vessel cover or bottom, may deliver unrealistic and non-conservative results with respect to creep damage.

Acknowledgements

The authors are obliged to the European Commission to participate in the project Reactor Vessel Integrity in Severe Accidents (REVISA) under contract F14S-CT96-0024. They are grateful to Dr T. Malmberg, Forschungszentrum Karlsruhe, Institut for Reactor Safety, for valuable discussions. The experimental work of Mr Eugen Groth is gratefully acknowledged.

References

[1] I. Tsagrakis, T. Malmberg, E.C. Aifantis, Review of experiments on similarity and size effects in uniaxial creep of smooth specimens, 22 February 2000, INV-REVISA(99)-P039.

[2] T.S. Mao, J. Granacher, C. Berger, Vergleichende Ermittlung des Zeitstand-verhaltens bauteilähnlicher Rundproben durch Versuche, Rissgefüge-beobachtungen und inelastische Finit-Element-Analysen, Schlussbericht zum Forschungsvorhaben DFG KI 300/54-1 und 2, 26 February 1999.

[3] A.K. Schmieder, Size effects in creep and rupture tests on unnotched and notched specimens of CrMoV steels, ASME Publ. 6–81, New York, 1974, p. 125.

[4] K.H. Kloos, J. Granacher, R. Tscheuschner, Schlussbericht zum Forschungs-vorhaben: Anriss- und Rissfortschrittsverhalten zeitstandbeanspruchter warm-fester Schmiedewerkstoffe DFG KI 300/30 und KI 300/46-2, 1986.

[5] K. Krompholz, J. Kamber, D. Kalkhof, A preliminary study of the material homogeneity for size effect investigations, PSI Bericht Nr. 99-03, June 1999, INV-REVISA(99)-P022.

[6] ASTM Designation: E139-95, Standard practice for conducting creep, creep-rupture, and stress-rupture tests of metallic materials, Ann. Book of ASTM Standards, Vol. 03.01, 1996, p. 252.

[7] F.H. Norton, The Creep of Steel at High Temperature, McGraw-Hill, 1929.

[8] Materialprüfnormen für metallische Werkstoffe 1, DIN-Taschenbuch 19. 11, Auflage 1989, Beuth Verlag, Köln, DIN 50 118, p. 93.